

LASER INTERFEROMETER GRAVITATIONAL WAVE OBSERVATORY
- LIGO -
CALIFORNIA INSTITUTE OF TECHNOLOGY
MASSACHUSETTS INSTITUTE OF TECHNOLOGY

Technical Note	LIGO-T1800224-v0	2018/10/25
Thermal State of Advanced LIGO Test Masses: Implementation of a Mirror Degradation Monitor Final Report		
SURF Student: Guadalupe Quirarte, Harvey Mudd College Mentors: Carl Blair, Joseph Betzweizer		

California Institute of Technology
LIGO Project, MS 18-34
Pasadena, CA 91125
Phone (626) 395-2129
Fax (626) 304-9834
E-mail: info@ligo.caltech.edu

Massachusetts Institute of Technology
LIGO Project, Room NW22-295
Cambridge, MA 02139
Phone (617) 253-4824
Fax (617) 253-7014
E-mail: info@ligo.mit.edu

LIGO Hanford Observatory
Route 10, Mile Marker 2
Richland, WA 99352
Phone (509) 372-8106
Fax (509) 372-8137
E-mail: info@ligo.caltech.edu

LIGO Livingston Observatory
19100 LIGO Lane
Livingston, LA 70754
Phone (225) 686-3100
Fax (225) 686-7189
E-mail: info@ligo.caltech.edu

1 Introduction

The Advanced LIGO (aLIGO) detector is composed of a Michelson interferometer with 4 km Fabry-Perot optical cavities that function as the arms of the interferometer. These cavities utilize high-reflectivity fused silica mirrors that form an optical cavity and interact with high power laser beams. These mirrors are referred as the input test mass (ITM) and the end test mass (ETM) of each arm as shown below in Figure 1. Each cavity has an optical power that ultimately will reach 800 kW. A small portion of this power is absorbed by test masses and then converted into heat. A thermal transient is created in the mirrors when the arm cavities control systems are locked attaining optical resonance in the arm cavities.

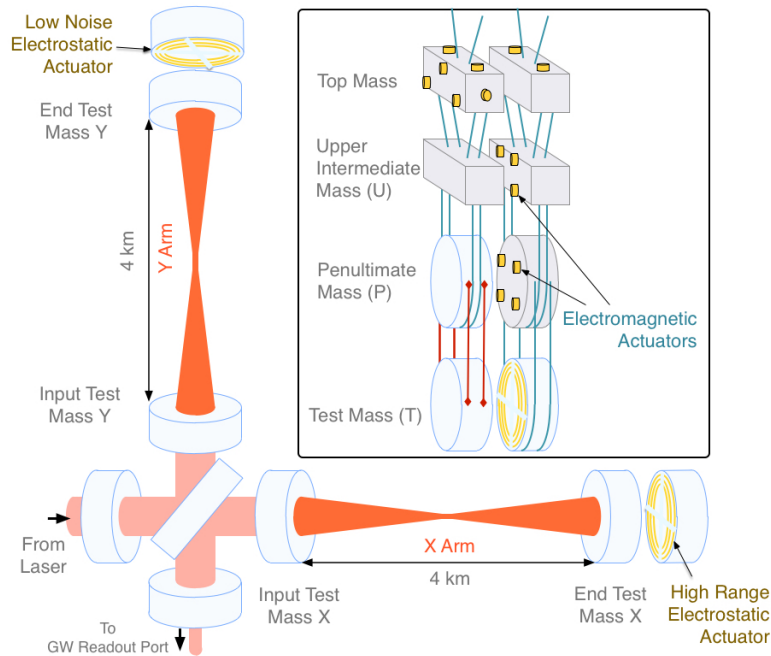


Figure 1: Diagram of an Advanced LIGO interferometer with Fabry-Perot cavities. [11].

This thermal transient's effect on the interferometer is dominated by two mechanisms. The first is known as thermal lensing which is caused by a change of refractive index through the thermo-optic effect. This thermal lensing can cause aberrations in the beam entering and leaving the detector's arm cavities that contribute to a deterioration of the mode matching between the many optical cavities of the interferometer which in turn reduces the sensitivity of the interferometer.[2]

The second effect is the high-reflectivity coatings of the test masses being deformed from thermal expansion. A change of the radius of curvature (ROC) of the mirror is the first order deformation and this shifts the frequency of the transverse optical modes (TEM) resonant in the cavity. This changes the tuning conditions for parametric instabilities. [2] As the mirror warms there is also a relatively small increase in the mechanical mode frequencies due to the small positive thermal dependence of the Young's modulus of the mirror substrates. Parametric instabilities arise when the frequency spacing between the fundamental mode and a TEM mode equals the mechanical mode frequency. The interferometer can become

inoperable and unstable if this condition is met.

These are problems that need to be addressed and investigated. Work has been completed by LIGO researchers to design and develop strategies aimed to compensate these thermal effects such that they do not impact the detector sensitivity. The paper, “Thermal modelling of Advanced LIGO test masses,” discusses how LIGO researchers have built a thermal model of the test masses that applies shifts in mechanical mode frequencies as a probe for the overall temperature of the mirror. This paper provides information on estimates of the coating absorption of the ETMY of the Livingston detector.[2]

LIGO researcher, Simon Tait, has worked with the thermal model outlined above in an effort to create an instantaneous absorption estimate of aLIGO test masses. He has modified the COMSOL thermal model and has written Matlab scripts that extract eigenfrequency and temperature data from the models. He has conducted parameterizations on the data to create an exponential model which he compared with experimental frequency tracking. The experimental frequency tracking integrates a transfer function and the extraction of the coating absorption. His final results focus on the month of July 2017. His code compares the simulated eigenfrequency of the test mass with the measured eigenfrequencies of the test mass. The eigenfrequencies are measured in the light in the transmission of the output mode cleaner. As there are several other contributions to the change in eigenfrequency, his code calculates the coating absorption by normalizing the gradient of this shift as the ratio of the measured and simulated gradient in eigenfrequency in the first two hours of lock. Shifts in the mechanical frequencies are tracked through this method during lock periods marked as stable for meeting a specific time threshold.[1]

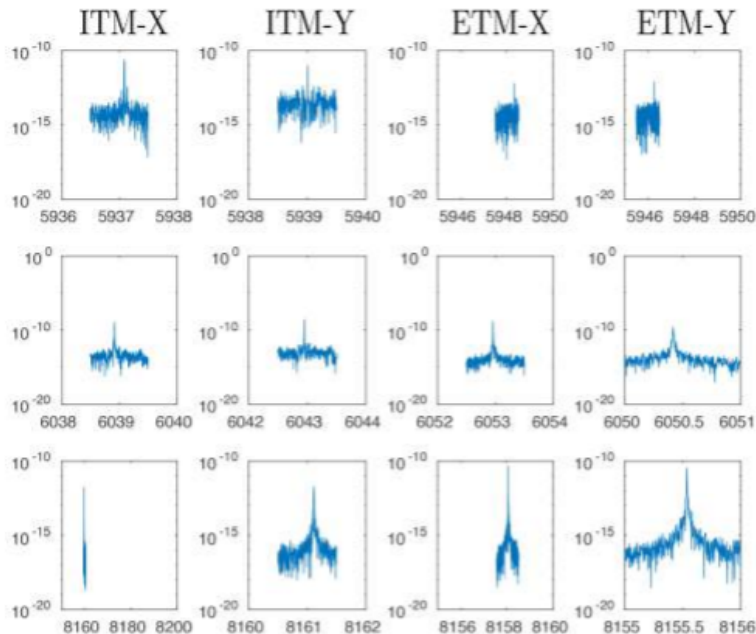


Figure 2: This is the windowed Power Spectral Density of the OMC output showing resonant frequencies of ITMs and ETMs in Hz. [1].

Tests have only been conducted between January and September of 2017. However,

further work that can be integrated is implementing a Kalman Filter into the LLO Thermal Compensation System monitoring system to help produce an instantaneous absorption estimate of the LLO test masses. This is what this project is focused on creating.

1.1 Motivation

The purpose of this project is to use the eigenmodes of the test mass to measure its thermal state. The ultimate goal is to build a Kalman Filter to optimally estimate the eigenfrequencies of the test mass. In the process of making this optimal estimate Kalman Filter, state space parameters will be updated which can be applied to track critical thermal compensation system parameters such as coating absorption.

1.2 Overview

This project involves working with COMSOL models and learning how to analyze and extract useful information from them. The LIGO CDS system was a necessary component for the extraction of data from the interferometer archives. Integrating the Kalman filter state space model parameters such as the test mass coating absorption can be inferred. This information was then used to optimize the thermal compensation, to minimize detrimental thermal effects on the interferometer.

The current work on this project involves the use of COMSOL model analysis built from the existing COMSOL Multiphysics models from S.Tait [3] and H. Wang [2]. The simulated eigenfrequency data from these models has been parameterized in preparation for building a Kalman filter state space model. Lastly, a Kalman Filter has been developed that estimates eigenfrequencies of the test mass that can be further tested on actual data.

Before explaining the work that has been done on building the Kalman Filter mirror degradation monitor, it is useful to have a background on mechanisms and work that has been completed beforehand. In the following sections, there is information on the essential components of the thermal compensation system, introducing the finite element model, the completed parameterization, and the Kalman Filter implementation.

2 Progress

2.1 Background

The following section describes the interferometer's Thermal Compensation System and the Pound Drever Hall technique utilized for locking the cavities. This is aimed to provide the sufficient background information of the mechanisms involved in producing thermal transients and also on extracting the eigenfrequency data for this project. This provides information about the control system inputs and outputs for the implementation of a mirror degradation monitor.

2.1.1 Thermal Compensation System (TCS)

aLIGO's Thermal Compensation System (TCS) is supposed to help mitigate optical distortion effects on the LIGO test masses.

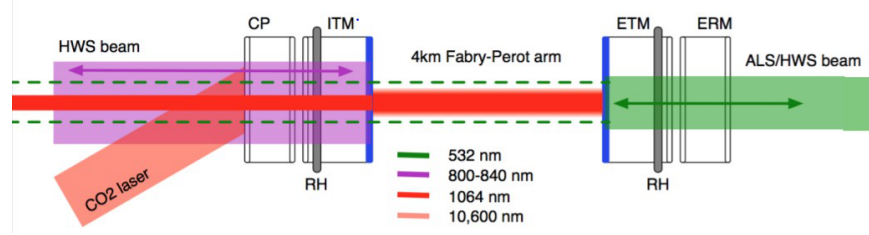


Figure 3: TCS system including Inner Test Mass (ITM), End Test Mass (ETM), circular ring heater (RH) to heat the test masses on the outside, a CO_2 laser projects various annular shapes onto the compensation plates, and the Hartmann Wavefront Sensor (HWS) [3].

The Ring Heater (RH) heats the test masses on the outside near the rear surface. This produces a negative thermal lens in the optic and decreases the radius of curvature of the concave mirrored surface of the test mass. The CO_2 laser heats an area in the center of the compensation plate, this produces a positive thermal lens. The HWS measures the wavefront distortion of the the HWS probe beam. This wavefront distortion is dominated by the thermal lens in the ITM and CP. The main purpose of this system is to compensate for the laser power absorbed in the test mass mirror coatings. [1]

The power absorbed into the optic is proportional to the input laser power P_{power} and α_λ the absorption at the wavelength of the laser. The formation of a thermal lens and thermal expansion are the two effects created by the thermal transient that forms when the cavities control system is locked producing a large laser power in the optical cavity, this locking process will be described below. Figure 4 provides a visual of a the thermoelastic surface deformation and wavefront distortion due to the thermal lens. The thermally distorted mirror, illustrated as a dashed line, shows the change of radius of curvature of the mirrors. This shifts the frequency of the transverse optical modes (TEM) resonant on the cavity by the order of $10^3 Hz$. This can dramatically, change the tuning conditions for parametric instabilities, inducing many different instabilities. The change in temperature of the optic results in a small shift in the mechanical eigenmode frequency of the test masses of approximately 0.2 Hz. If the shifted frequency of the TEM modes and the spacing to the fundamental central mode of the cavity become equal to the frequency of the mechanical modes, then the radiation pressure of the optical modes can result in an exponentially increasing excitation of the mechanical modes known as parametric instability (PI) leading to the unlocking of the cavity. [1]

The cavities are locked through the Pound Drever Hall (PDH) technique. A basic layout for locking a cavity to a laser is depicted below. The Pound Drever Hall technique also provides a means of measuring the length of noise of the optical cavity. The main mechanism behind the setup can be divided into three steps. A beam is sent into the cavity, a photodetector takes in the reflected beam, and then its output goes to a length controlling

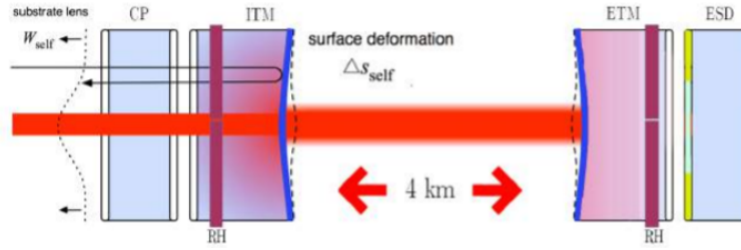


Figure 4: Thermoelastic surface deformation (Red beam representing laser beam heating causing deformation of inner and end test masses, visually exaggerated.) [3].

actuator. With a correct feedback setup, the system will hold at the length of the cavity where light is resonant.[10]

However, the actual PDH technique is more complex. Before the beam is sent into the cavity, it is frequency modulated with Pockel cells as depicted in Fig. 5. Through this modulation, sidebands are produced that can be visualized as three distinct frequencies being incident upon the cavity. These distinct frequencies include the upper sideband frequency, the original laser light, and the lower sideband frequency. The sideband will not be perfectly resonant when the cavity is in resonance with the main laser light. When there are perturbations in the cavity, one sideband will approach resonance while the other will diverge from resonance. This creates an imbalance in the sidebands reflected from the cavity. An error signal is then created that reflects the sidebands. This error signal's purpose is to control the optical cavity length. This involves demodulating the signal with the original LO modulation frequency and then low pass filtering the signal with servo amp which passes only the low frequency information. [10]

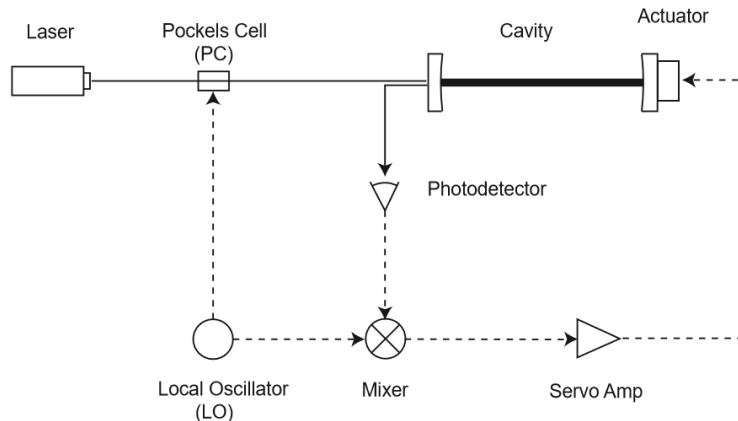


Figure 5: Locking a cavity to a laser. (Dashed lines are signal paths and solid lines are optical paths) [10].

When the cavity is resonant, it also experiences a large laser power build up. A portion of the light is absorbed in the high reflectivity optical coating. Currently, the detectors have design specifications for ETM coatings to have an optical absorption of 0.5 ppm and 99.999

reflectivity at 1064 nm. [1] The input mirror is more complicated as the reflectivity is formed by the ITM and another mirror PRM forming a coupled cavity. The resulting resonance results in 4000x more light in the arm cavity compared to the input light. The small portion of this light that is absorbed in the coating dominates the thermal load on the test mass resulting in the deformation as pictured on Figure 4.

As described above, heat loads are generated in the test masses and the thermal compensation system is used to compensate for these heat loads. The next section will describe in detail the affects heat loads have on the test masses. This also helps further understand the next steps of the project which involve the thermal analysis of the test masses and the development of the degradation monitor.

2.2 Final Element Model

This section focuses on the development of a model of the entire thermal system utilizing COMSOL Multiphysics. The objective of the following procedures is to provide a parametric model of the shift in eigenfrequencies. The results from this section provide parameters that are used as inputs for the mirror degradation monitor Kalman Filter.

2.2.1 Method

Mechanical mode frequencies have been described as test mass thermometers.[2] They depend on the dimension of the test mass and on two material properties with a temperature dependence. These properties are the Young's modulus and the Poisson ratio. [2] An analytic way to express the eigenfrequencies of a cylinder is by following the equation below.

$$\omega_m = \beta_m \sqrt{\frac{Y(T)_{bulk}}{\rho(1+\nu)}}$$

Equation 1. The Mechanical Mode Frequency [3]

As shown above, the mechanical mode frequency ω_m is directly proportional to the square root of the Youngs modulus $Y(T)_{bulk}$ and inversely proportional to the material density ρ and the Poisson ratio ν . The variable β_m is corresponding to a constant dependent on the geometry of the cylinder.

2.2.2 Thermal Model

A thermal model of the test mass allows the temperature distribution in the test mass to be estimated for a particular thermal load on the test mass. This thermal model includes the test mass and its surrounding bodies. The accuracy of the aLIGO test mass thermal model can be improved by including thermal coupling. This is done by including the radiative heat transfer between the test mass and the other bodies surrounding it, which are discussed in section 2.1.1 under TCS. [2]

The model above illustrates the mechanisms involved during the transfer of heat when an arm cavity is locked. A portion of the light is converted into heat and scattered light from the beam covers bodies surrounding the test mass. Longer time constants are introduced

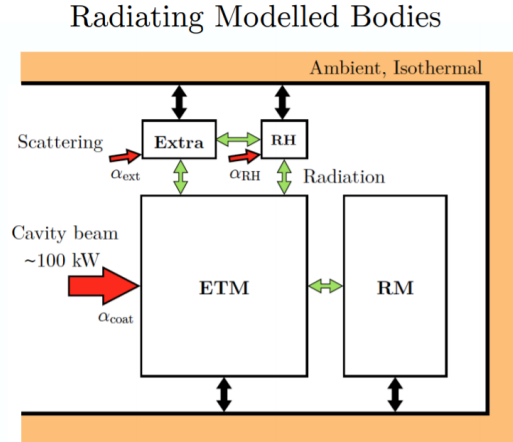


Figure 6: This is a heat transfer model between an end test mass and its surrounding elements, Ring Heater (RH), a reaction mass (RM), and the extra term represents other complex structures surrounding it. The red arrows represent the energy coming from the intra-cavity beam through scattering and coating absorption. The green arrows represent the energy from radiative heat coupling between different components. The black arrows represent the radiative heat coupling with the surroundings (ambient) A way of improving the accuracy of the thermal modelling is through the incorporation of the radiative heat transfer between the mirror and components at close proximity. [3].

to the test mass thermal transient because some of the heat from absorbed light radiatively couples to other structures. This object's increased temperature then radiatively couples heat back to the test mass.[2]

2.2.3 COMSOL

A state space model is required for the development of a Kalman Filter. It is a mathematical model that takes a set of input, output, and state variables of a physical system. To create a state space model of the test mass eigenfrequencies an accurate thermal model is required. The COMSOL Multiphysics heat transfer toolbox was utilized to perform this thermal modelling. An end test mass was modelled, ETMY (test masses are nominally identical), and studies were ran pertaining to its acoustic modes. The heat transfer module was attached to calculate the temperature of the ETM over time. A solid mechanics study is also attached to the module calculating eigenfrequencies of the ETM over time.

An aLIGO test mass is a cylinder with a 170 mm radius and 200 mm thickness made of Heraeus Suprasil 3001 fused silica.[4] When a 100 kW laser beam is shot at the system, the model utilizes a heat source boundary condition with a Gaussian profile to simulate the area in which the beam hits the mirror surface as shown in figure 10. With a laser beam of this power, the coating absorption of 1 ppm would correspond to a total absorbed energy of 0.1 W. The only input of the model that is given to it is the laser power step function. When the cavity is unlocked it is 0 and when the cavity is locked the measure power is 0.1 W. Figure 7 depicts the inputs and outputs of this thermal model and figure 8 provides a

visual of the 2 dimensional thermal model of the whole system. [2]

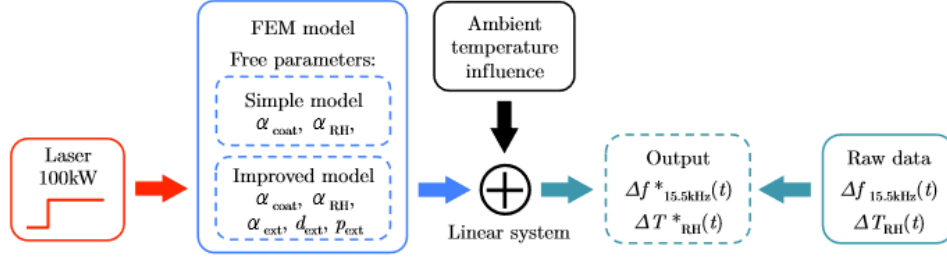


Figure 7: A finite-element model showing the inputs, outputs, and the free parameters to take into account when modelling a test mass. The red arrow represents the input laser power, combined with the varied free parameters in blue, and the ambient temperature influences in black which are all inputs in a linear system. As illustrated above this is then further combined from the right with raw data (one can obtain eigenfrequency data) to then obtain output eigenfrequency shift results. [2].

By running the physics, setting the material properties, and running a time dependence and eigenfrequency study, H. Wangs [2] model was used as a guide to learn how to navigate through the program. The focus was testing the behavior of fused silica. Fused silica has a unique behavior as its Youngs modulus increases with temperature over some temperature range. As shown in the previous section, Youngs modulus is directly related to the mechanical mode frequency. Wang’s model shows a rise in frequency of the mechanical modes of the material when applying a heat load. This heat load creates an increase in temperature of the mirror which in hand increases the mechanical mode frequency. Below is a table of the material properties modelled for this material.

Material Property	Symbol	Fused Silica	Unit
Density	ρ	2203	$\frac{kg}{m^3}$
Poisson’s Ratio	ν	0.17	1
Young’s Modulus	E	$(7.3 \times 10^{10})(\Delta T)$	Pa
Thermal Conductivity	κ	1.38	$\frac{W}{mK}$
Thermal Expansion Coefficient	α	5.5×10^{-7}	$\frac{1}{K}$
Heat Capacity	C_p	740	$\frac{J}{kgK}$
Relative Permittivity	ϵ	3.8	1
Electrical Conductivity	σ	1×10^{-14}	$\frac{S}{m}$
Surface Emissivity	ϵ_e	0.93	1

A thermal modelling simulation was conducted by adding a theoretical heating load

and 8kHz modes. These modes have been analyzed with a 3D geometry model. The 5.9 and 6.0kHz modes are not axis-symmetric. The 8kHz mode is axis-symmetric, as a result the rest of this report will focus on the 8 kHz mode.

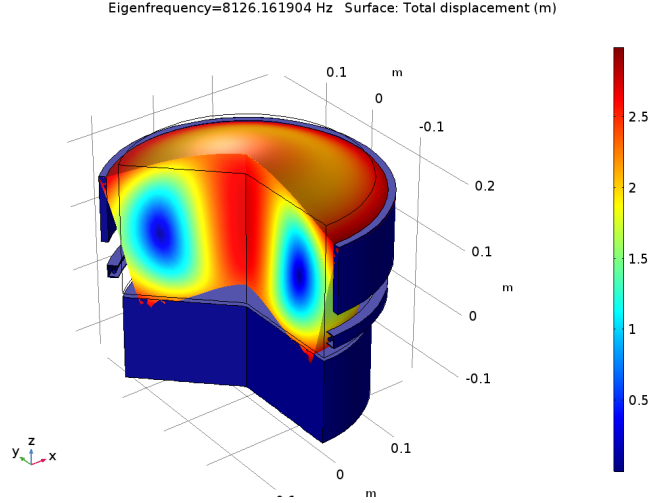


Figure 9: Mechanical mode shape of the 2DAS modelled ETM surrounded by the Ring Heater, ERM and an approximated suspension. The variance in color only present on the end test mass highlight the eigenmode shape created with the laser heating load applied on the end test mass. The surrounding elements including RH, RM, and the Extra Term as described from figures 6 and 8 are not included in the mechanical mode shape formed from the heating and as a result are depicted in dark blue. [1].

An aLIGO interferometer's arm cavity contains a 100kW Gaussian beam centered in the cavity. The equation below shows how the power absorbed by the optic, P_α , is calculated. The ω corresponds to the beam radius of the incident Gaussian light source and the value is 6.2 cm, the r refers to the distance from the center of the beam. P_{in} is the power input into the Fabry Perot cavity, k_{PRC} is the gain of the power recycling cavity, and k_{AC} is the gain from the arm cavity.[1]

$$P_\alpha = \frac{2(P_{in}k_{PRC}k_{AC})}{(\pi\omega^2)} \exp\left(\frac{-2r}{\omega^2}\right) \frac{1}{\alpha_c}$$

Equation 2. Power absorbed by the optic [1]

The α_c is the absorption of the coating on the test mass and it has been measured to be approximately 1.4 ppm at 1064 nm by using a Hartman Wavefront Sensor (HWS) for ETMY.[1] Furthermore, while analyzing the model, one can notice how the shift in ETM mechanical mode frequency was observed with relation to the surrounding optics in over 40 hours. By adding more components to the simulation this produces an elevation in re-radiation effects from the addition of these bodies. As a result, there is an increase in the calculated change in frequency over time [1].

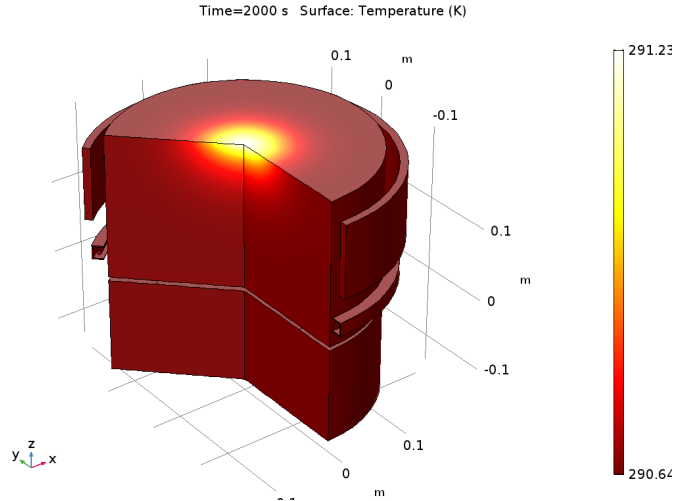


Figure 10: The COMSOL model above portrays the end test mass system with its surrounding elements (RH, RM, and Extra Term) to illustrate the temperature behavior of ETM when a heating load (representative of the main laser beam) of approximately 100 kHz is applied to the system. The change in the color has a radially outward changing direction which depicts the radial temperature gradient of the optic. [1].

2.3 Model Parameterization

With a clear understanding and analysis of COMSOL, the curve fitting exponential model described in S. Tait [1] was derived. By using MATLAB to obtain the COMSOL data of the eigenfrequency shift of the specific eigenmode 8.126 kHz, one can obtain the modelled shift of the frequency. COMSOL provides a finite element model data used as a fit to create a parametric model. The goal is to extract a good fit of this analytical model and to obtain an exponential model. The next section explains how this model can be applied for the Kalman Filter.

The equation below is one of the fits for frequency change in temperature calculated with COMSOL. This is a single term exponent with respect to time. The A corresponds to the total change in frequency, b_1 is the model time constant, and c_1 is the frequency at room temperature. This model can then be used to produce a simulated absorption estimate.

$$A(1 - e^{-b_1 t}) + c_1 \quad \text{Equation 3. Exponential Model [1]}$$

Prior to extracting the data through the MATLAB interface, the original COMSOL model experienced modifications. The model was clarified by adding descriptions to the parameters and variables to allow other future users to have an understanding of the derivation of these components. A major modification made was removing the frequency shift produced by cooling and only keeping the heating transient as it simulates a locked state. As described by Wang [2], this model can be approximated as a linear time invariant system. By removing the cooling transient, one could obtain a set of frequencies for a specific eigenmode. Simon's code produced an estimate for the change in temperature and frequency with self-heating from his pre-solved COMSOL model.

Before extracting the eigenfrequencies, it is important to extract the temperature difference from the model for all the ETM points. Plotting provides the possibility of graphically analyzing whether the data highlights reasonable heating behavior. The graph below illustrates the heating transient formed for all four bodies modelled.

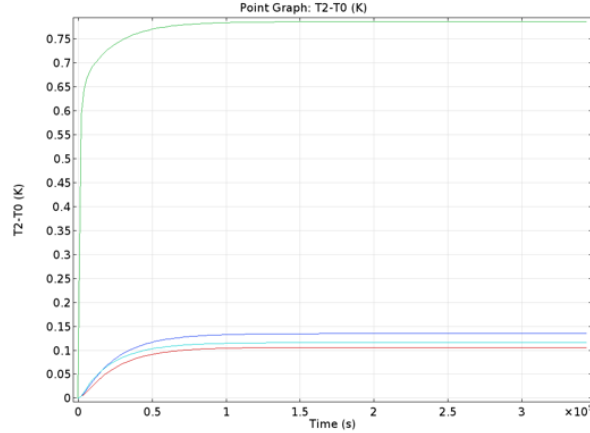


Figure 11: **Graph 1:** The graph above can be obtained by plotting on MATLAB the temperature over time of the end test mass and the other bodies to observe the behavior to model the heating of the masses. The different colored lines represent the five distinct eigenmodes being modelled on COMSOL. [1].

Once the plot for Graph 1 was completed, the loop was ran through the data for the specific eigenmode. The curve fitting tool from MATLAB was then applied to work on fitting the analytical data to a second-degree exponential model to see if it provided a better fit to the data. As explained in section 2.2.2, thermal coupling must be taken into account when creating a thermal model. As a result, the model was changed to see if longer time constants were introduced. This could represent how some of the heat from scattered light radiatively couples to other elements.

$$A(1 - 2e^{-b_2t} + e^{-2c_2t}) + d_2 \quad \text{Equation 4. A Test Exponential}$$

Model

The gain A was approximately 0.09, the time constants b_2 and c_2 were 0.159 and 0.079, and d_2 the eigenfrequency at room temperature was 8126. While fitting the model, the lower and upper limits were kept large to ensure the data was not being forced to fit a specific mold. Although the goodness-of-fit statistics obtained for both this model and the original model were very similar and the r squared was approximately 0.9936-0.9958, the first data point at time zero did not match the exponential model. By forcing d to be the y-intercept value of 8126.17, this would result in a less fit model of the function and would require a forcing of the variables b_2 and c_2 .

Below is a graph of the curve fitting model with the value obtained for b_2 and c_2 previously stated. Both the first order exponential model and the second order exponential model provide closely similar values for the goodness-of-fit statistics. In order distinguish which exponential model is best to apply for the Kalman Filter, both models need to be

examined. This would require applying each one separately in the implementation of the filter. Afterwards, one can analyze which assumed model provides the most reasonable coating absorption estimates. Currently, the first order exponential model was applied as an input for the mirror degradation monitor. Further work can be done by applying the second order exponential model instead to compare which curve fit model is best to apply for the monitor.

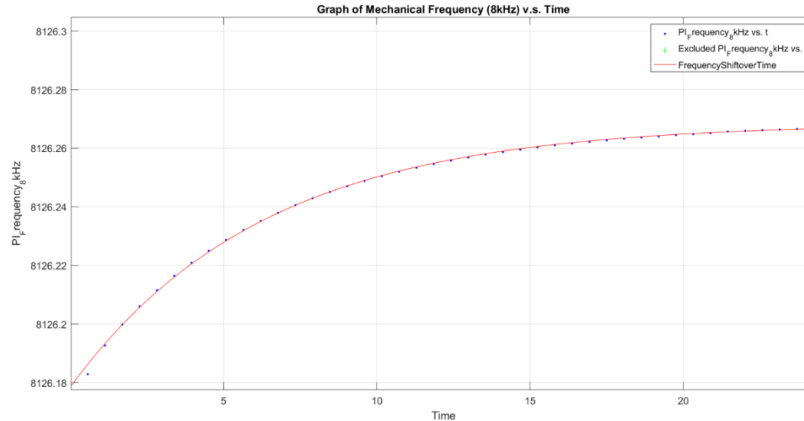


Figure 12: **Graph 2:** Exponential Model curve fitting of the numerical data from COMSOL. This graph illustrates the finite element modelling data in blue obtained from COMSOL and the red line is the parametric model fit obtained applying the finite element model data (blue dots). [1].

2.4 Calculated Coating Absorption

This section focuses on the results obtained by Simon for the period of January through September 2017 with estimates of the coating absorption.[1] The purpose of this section is to investigate the previous methods used to investigate coating absorption such that the Kalman Filter method can be contrasted and compared to this previous method.

The following graphs show Simon’s results of calculated coating absorptions during this time period. Since the eigenfrequency data can only be measured from the OUTPUT mode cleaner during lock states, the unlocked state estimates were produced by applying the method of interpolation. This method constructs data points for the unlock state within the range of the discrete set of known eigenfrequency data and following the inverse behavior of a lock.

A prediction of the coating absorption was made, using the equation below,

$$\alpha_{coat} = \frac{\Delta f_{meas}}{\Delta f_{sim}} \alpha_{sim}$$

Equation 5. Coating Absorption [1]

where the numerator is the gradient of the measured frequency shift with time and it takes into account both locked and unlocked states. The denominator is the simulated change in frequency. The code to complete this coating absorption estimate was run for the month of

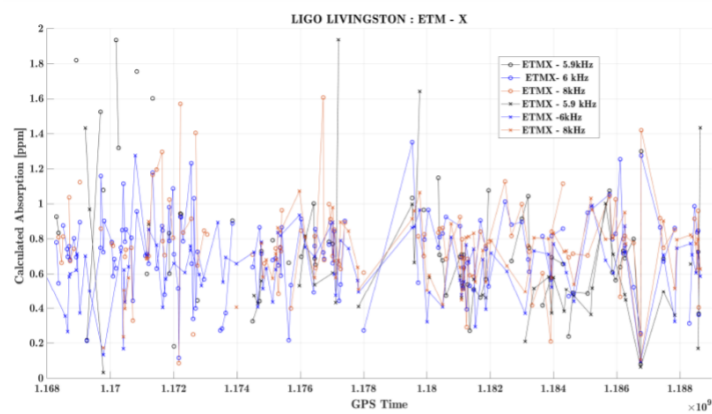


Figure 13: The calculated optical absorption during locked and unlocked states of ETMX between January and September of 2017. \circ refers to locked times and \times is the interpolated estimate for the unlocked states. The different colors and line shapes are indicative of the three eigenmodes 5.9kHz, 6kHz, and 8 kHz being tested for the End Test Mass of the X arm. [1].

July and the approximation was reasonable. It can be used to model both ITM and ETM. Although an understanding of this instantaneous coating absorption extraction technique is ideal for further comparisons, this project focuses on creating a different method of extracting the coating absorption through the implementation of a Kalman Filter.

2.5 Kalman Filter Implementation

2.5.1 Kalman Filter Theory

A Kalman Filter is a recursive algorithm that takes in as input a model and measurements to output less noisy and more accurate estimates. This filter is ideal for real time problems since it has the advantage of only taking in the previous state of the system and not requiring any other history. The figure below provides a clear overview of the mechanism behind the algorithm and its functionality. It is widely used in different areas such as navigational systems, guidance, and controlling vehicles. [5]

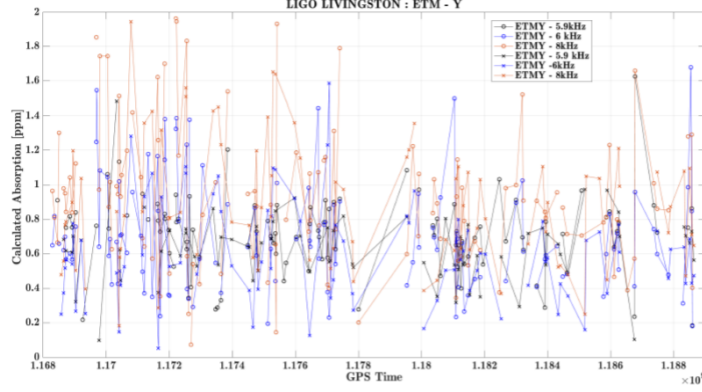


Figure 14: The calculated optical absorption during locked and unlocked states of ETMY between January and September of 2017. o refers to locked times and x is the interpolated estimate for the unlocked states. The different colors and line shapes are indicative of the three eigenmodes 5.9kHz, 6kHz, and 8 kHz being tested for the End Test Mass of the Y arm. [1].

The application of a Kalman Filter for an internal system requires the use of the state-space representation of this system. The equation below illustrates how the present state is dependent on the previous state.

$$\mathbf{x}_k = \mathbf{A}_k \mathbf{x}_{k-1} + \mathbf{B}_k \mathbf{u}_k + \mathbf{w}_k \quad \text{Equation 6. [5]}$$

\mathbf{A}_k represents the state transition model used to the previous state \mathbf{x}_{k-1} and \mathbf{B}_k represents the input-control model. The input-control model is applied to the control-vector \mathbf{u}_k and the state matrix is applied to the state-vector \mathbf{x}_{k-1} . The process noise is represented by w_k which in this case is a univariate normal distribution with covariance \mathbf{Q}_k . [5]

$$\mathbf{z}_k = \mathbf{C}_k \mathbf{x}_k + \mathbf{v}_k \quad \text{Equation 7. [5]}$$

Once the observation, \mathbf{z}_k (measurement), is taken representing the true state \mathbf{x}_k , as shown above, \mathbf{C}_k represents the observation model which is applied to the state vector at time k. Taking account of the measurement noise, \mathbf{v}_k , signifies the zero mean univariate normal distribution noise in this case with covariance \mathbf{R}_k . The observation is not affected by the control vector and as a result \mathbf{D}_k , the output-control model is equal to zero.

There are two variables that represent the state of the filter which are $\hat{\mathbf{x}}_{k|k}$ known as the a posteriori with an estimate at time k, and $\mathbf{P}_{k|k}$ which is the a posteriori error covariance matrix. The notation of these states can be described as $\hat{\mathbf{x}}_{a|b}$ where a is the time of the estimate and b is the time of the observation and b is restricted to be less than or equal to a. Below I have divided the Kalman Filter into two sections as it is normally explained in two phases: prediction and correction. [5]

Prediction

$$\hat{\mathbf{x}}_{k|k-1} = \mathbf{A}_k \hat{\mathbf{x}}_{k-1|k-1} + \mathbf{B}_k \mathbf{u}_k \quad \text{Equation 8. [5]}$$

$$\mathbf{P}_{k|k-1} = \mathbf{A}_k \mathbf{P}_{k-1|k-1} \mathbf{A}_k^T + \mathbf{Q}_k \quad \text{Equation 9. [5]}$$

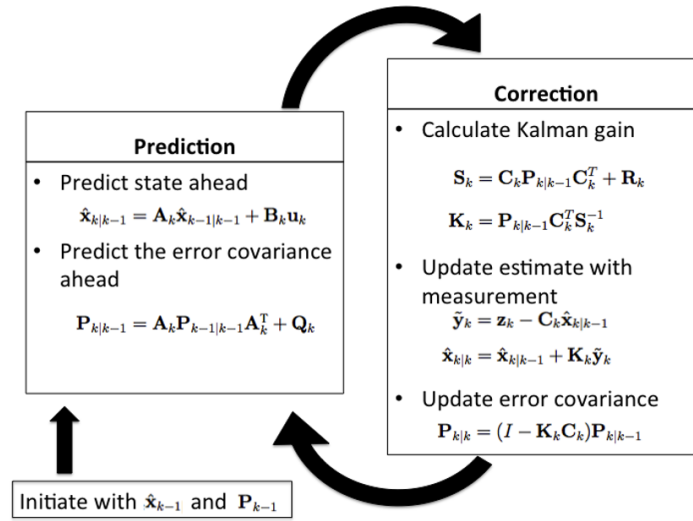


Figure 15: Kalman Filter thinking process. [5].

The prediction phase depends on the time-step's previous state as illustrated above. The predicted state $\hat{\mathbf{x}}_{k|k-1}$ is known as the a priori state estimate as it depends on the observation at time k-1. $\hat{\mathbf{P}}_{k|k-1}$ is the prior state covariance matrix. [5]

Correction

Calculating Kalman Gain:

$$\mathbf{S}_k = \mathbf{C}_k \mathbf{P}_{k|k-1} \mathbf{C}_k^T + \mathbf{R}_k \quad \text{Equation 10. [5]}$$

$$\mathbf{K}_k = \mathbf{P}_{k|k-1} \mathbf{C}_k^T \mathbf{S}_k^{-1} \quad \text{Equation 11. [5]}$$

Updating Estimate with Measurement:

$$\tilde{\mathbf{y}}_k = \mathbf{z}_k - \mathbf{C}_k^T \hat{\mathbf{x}}_{k|k-1} \quad \text{Equation 12. [5]}$$

$$\hat{\mathbf{x}}_{k|k} = \hat{\mathbf{x}}_{k|k-1} + \mathbf{K}_k \tilde{\mathbf{y}}_k \quad \text{Equation 13. [5]}$$

Update Error Covariance:

$$\mathbf{P}_{k|k} = (\mathbf{I} - \mathbf{K}_k \mathbf{C}_k) \mathbf{P}_{k|k-1} \quad \text{Equation 14. [5]}$$

The correction phase requires the calculation of the Kalman Gain as shown in equations 10 and 11 and then the updating of the estimate state by using the measurement. Moreover, the estimate state and the error covariance are updated by observing from the current time-step rather than the previous step.

2.5.2 Building a Kalman Filter

The following steps outline an approach towards building a Kalman Filter. These are the steps I have followed while moving forward in the project. [6]

1. **Understand the situation:** Look at the problem and break it down to the mathematical basics.
2. **Model the state process:** Starting with a basic model with one input and one control parameter, then in the future one can implement more input and control parameters to improve the Kalman estimate.
3. **Model the measurement process:** Analyze how you are going to measure the process.
4. **Model the noise:** This has to be completed for both the state and measurement process. The base Kalman filter assumes Gaussian (white) noise, so make the variance and covariance (error) meaningful (i.e., make sure that the error you model is suitable for the situation).
5. **Test the Filter:** Observe the behavior of the filter.
6. **Refine the Filter:** Try to change the noise parameters, if necessary go back and rethink the situation.

[6]

3 Preliminary Results

3.1 Practice Kalman Filter

Going through a Kalman Filter tutorial can help one develop a clearer understanding of the process before building the project monitor. A practice Kalman Filter tracking the two-dimensional position of an object using Matlab has been implemented. The appendix provides a detailed explanation of this tutorial highlighting the situation, state process, and analysis of testing and tuning the filter. This is a useful learning experience for anyone interested in gaining expertise in Kalman Filter theory and application.

3.2 Coating Absorption Estimate Kalman Filter

After completing a practice Kalman Filter and gaining deeper insight into the steps involved within the recursive algorithm, the project's next step was implementing a mirror degradation monitor. The ultimate goal of this project is to create a real-time monitor that extracts estimates of the coating absorption while applying Kalman Filter theory.

3.2.1 Approach

With the first order exponential model described in section 2.3 and the detector's eigenfrequency measurements for a set period of time, the approach is to first create a Kalman Filter with simulated data and then test it. The model below is the normalized exponential that will be used for the state-space representation. After completing the testing of the filter, the next step was the extraction of the coating absorption and transition into the actual implementation of real data.

$$f(t) = \mu(1 - e^{-\frac{t}{\tau}}) \quad \text{Equation 26.}$$

3.2.2 State-Space Representation

To create the state-space representation one must first understand that we are taking a physical system as a set of input, output, and state variables. These components are related by first-order differential equations which were found by starting with the unit step response of the system given by the model above. [5]

$$\begin{aligned} \mathbf{f}(s) &= \mathcal{L} \{ \mu(1 - e^{-\frac{t}{\tau}}) \} \\ &= \frac{N}{s^2 + Ds} \end{aligned} \quad \text{Equation 27.}$$

The Laplace transform operator \mathcal{L} was taken and applied to the analytical model to obtain the expression above where the coefficients N and D correspond to the following variables,

$$N = \frac{\mu}{\tau} \quad D = \frac{1}{\tau} \quad \text{Equations 28 and 29.}$$

The transfer function of the system is then given by taking,

$$\frac{\mathbf{f}(s)}{P(s)} = \mathbf{sf}(s) = \frac{N}{s+D} \quad \text{Equation 30.}$$

The inverse Laplace transform of the transfer function was then taken which ultimately results in giving us the differential equation.

$$\begin{aligned} \mathcal{L}^{-1} \{ \mathbf{f}(s)(s+D) = P(s)N \} \\ \dot{f}(t) + Df(t) = Np(t) \end{aligned} \quad \text{Equation 31.}$$

The differential equation above was applied to show the state-space representation of the system as depicted below where Δk corresponds to the sampling period and z_k is the observation measurement and is a variable of interest. [5] The model below illustrates how we are working with a one degree of freedom system.

$$[f_k] = [1 - D\Delta k][f_{k-1}] + [N\Delta k][P_k] \quad (32)$$

State-Matrix:

$$A = [1 - D\Delta k]$$

Input-Control Matrix:

$$B = [N\Delta k]$$

Measurement-Matrix:

$$C = [1]$$

Observation Model:

$$z_k = f_k \quad (33)$$

3.2.3 Parameters and Coefficients Estimation

With the state-space representation above, the following table shows the values of the parameters and the coefficients. The parameters were obtained as outlined in the previous section by creating a parameterization of the COMSOL data through Matlab.

Gain(μ)	0.8114 Hz/W
Tau (τ)	6.289 Hrs
N	0.129 Hz/(Hrs)(W)
D	0.159 Hrs ⁻¹

Table. 2.

3.2.4 Simulated Simple Kalman Filter Results

After completing the Matlab script with the given parameters, coefficients, and the state-space model described in section 3.2.2, I started by simulating a locked state. The control-input laser power is acting as a step function providing 0.1 W of power to the system. The graph below illustrates the shift in eigenfrequencies during the simulated lock with a comparison between the analytical model derived in section 2 with noisy eigenfrequency measurements.

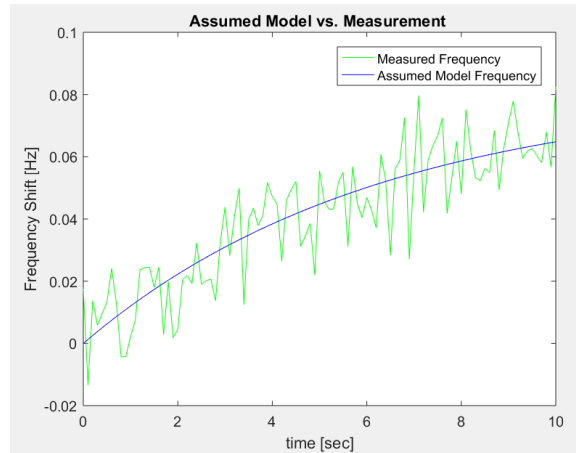


Figure 16: Simulated Lock State with the analytical model and simulated noisy measurements. The blue line is the assumed model frequency obtained in the previous section as the parameterized model. The green line is a simulation of measured frequency data obtained by adding noise to the model data.

Once the Kalman Filter runs through the time interval and goes through the noisy measurements comparing them to the analytical model, the following graph depicts how the Kalman estimates compare to the measurements.

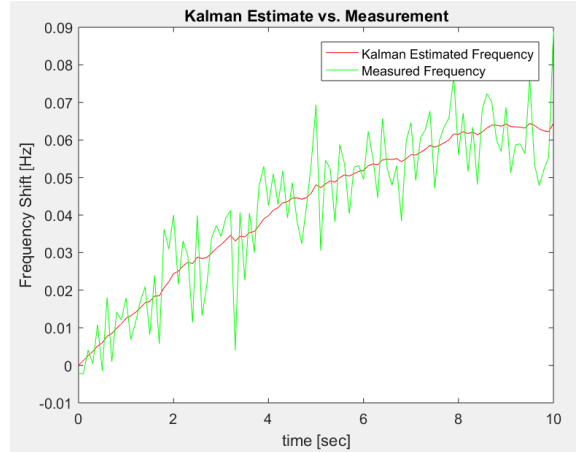


Figure 17: Simulated Lock State with the Kalman estimates from the MATLAB code and simulated noisy measurements. The red line represents the obtained Kalman estimate outputs from the Kalman Filter. The green line represents the simulated noisy measurements.

This is how the monitor should ideally function as it runs through real-time eigenfrequency measurements, but the goal of the project is to extract estimates of the coating absorption. The project faced a problem when realizing that this extraction would not be as efficient as first intended to.

3.2.5 Problem Extracting Coating Absorption

After completing the Kalman Filter, I arrived at a problem when reasoning through my strategy of extracting the coating absorption. Some questions that should have been thought of during the state-space representation process and while analyzing the situation include,

- Is there a parameter in the state space model that is proportional to the coating absorption?

In our case, the parameter associated with the coating absorption is the gain found in the exponential model defined as μ . With this parameter, I then need to review the following questions.

- Is it possible to obtain the state-space representation of the gain? [5]
- Can I implement a Kalman Filter with the state-space of the gain? [5]

In order to obtain the state-space representation of the gain, this parameter must have a linear relationship to the system. The current state vector is one degree of freedom and even though if I were to change it to two degrees of freedom it cannot include the gain. The gain needs to be linearized in order to implement the Kalman Filter. The common Kalman Filter only applies for linear systems. However, there is a version of a nonlinear Kalman

Filter known as the Extended Kalman Filter which linearizes around the current mean and covariance. The issue with this type of filter is that it can result in high computational costs. [5]

The problem with the current Kalman Filter is that the Kalman Estimate Gain does not update itself. When simulating a noise in the measurements that would be representative of the change in coating absorption, the Kalman estimate does not update. This is due to the fact that the gain is found within the input-control matrix, B , as outlined in section 3.2.2. The input-control matrix in the Kalman Filter algorithm remains unchanged. During a lock state, when the laser power is nonzero at approximately 0.1 W, the coating absorption is correlated to the laser power. Due to this relationship which is described in the COMSOL section 2.2.3, the actual eigenfrequency measurements for the 8 kHz eigenmode are assumed to contain this with variation in coating absorption. However, the Kalman estimate does not update itself due to this noise in the measurements.

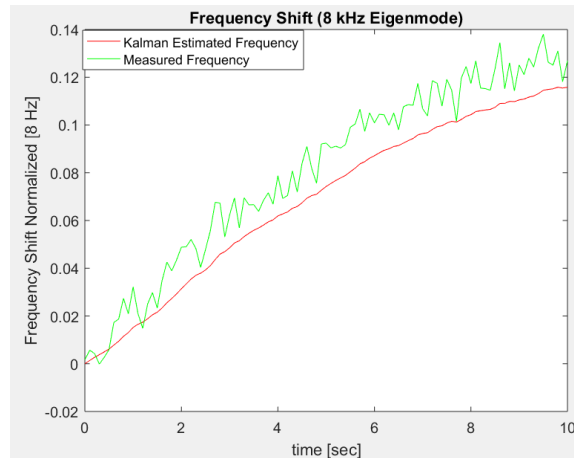


Figure 18: Simulated Lock State where the actual noisy measurements have a factor of 2 multiplied to the input laser power and the Kalman Estimate is not updated. The green line represents the noisy measurements with an implemented bias (modelling the dependence on other factors such as ambient temperature [explained in the introduction section]). The red line represents the output eigenfrequency estimate from the Kalman filter.

The following two graphs illustrate the problem. Figure 23 depicts an example where the measurements have an extra factor added to the input laser power. It changes the gain coefficient in the measurements as this noise increases the laser power's effect and can be analyzed as the coating absorption's effect. The problem is that the Kalman Estimate's gain coefficient remains unchanged with this measurement noise. Figure 24 below applies the same analysis, but in this case the Kalman Estimate's gain is greater than the measurements. The measurements have a noise simulating an effect where there is a factor reducing the laser power's effect. Once again, the Kalman Estimate does not experience a reduction in gain to match the behavior of the noisy measurements. Although both the Kalman Estimate and the noisy measurements graphs eventually converge to the same value during a lock, the difference in the early behavior of a lock is a problem since the coating absorption extraction is dependent on analyzing this time interval.

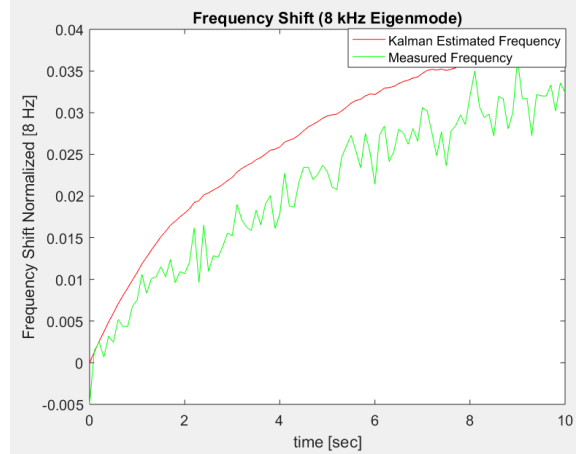


Figure 19: Simulated Lock State where the actual noisy measurements have a factor of .5 to the input laser power and the Kalman Estimate is not updated. The green line represents the noisy measurements with an implemented bias (modelling the dependence on other factors such as ambient temperature [explained in the introduction section]). The red line represents the output eigenfrequency estimate from the Kalman filter.

3.2.6 Creating a Nested Kalman Filter

The approach taken in order to monitor and change the gain of the Kalman Estimate was centered on creating a nested Kalman Filter. Although the gain can be linearized, due to the time constraint of the project, this measure will be postponed for later.

Applying the original Kalman Filter created for this system as the basis of the nested filter, the strategy behind this more complex monitor involves updating the input-control model, B , and the process covariance at the end of each lock state. Since the process covariance is directly proportional to the product of B and its transpose, by updating B the process covariance changes as well. As explained in the previous section, the gain is directly related to B . At the end of a lock state, the Kalman Estimate will either be above or below the measurement data as illustrated in figures 23 and 24. By measuring the average residual during this time frame between the measurement and the Kalman Estimate, this is then factored to the input-control model. The outer Kalman Filter is a simplified Kalman Filter where the model noise standard deviation, w , and the measurement noise standard deviation, v , are set at a value with no time evolution. As a result, one currently cannot provide estimates of the process covariance, Q , and the measurement covariance, R .

$$B_{updated} = B_{initial} + (\text{average residual}) * B_{initial} \quad \text{Equation 34.}$$

The equation above explains how the input-control model is updated at the end of each lock period. The gain is then updated at the end of each lock period and graphed separately to illustrate the change as the detector alternates between locked and unlocked states. With a larger sampling time, the gain can be updated to the point where the Kalman estimates' gain is closer to the actual measurement gain. After completing the Matlab code which implements this simplified nested Kalman Filter, it was tested with a simulated time frame of alternating locked and unlocked states to test two cases.

Simulation Results:

The first case involves encountering noisy measurements where the control parameter, laser power, has an unknown factor greater than 1 resulting in a higher gain coefficient in the measurement data. As shown below, the nested Kalman Filter updates itself at the end of locked states to update its gain coefficient. This results in an increase in the gain and this change in gain is proportional to the coating absorption.

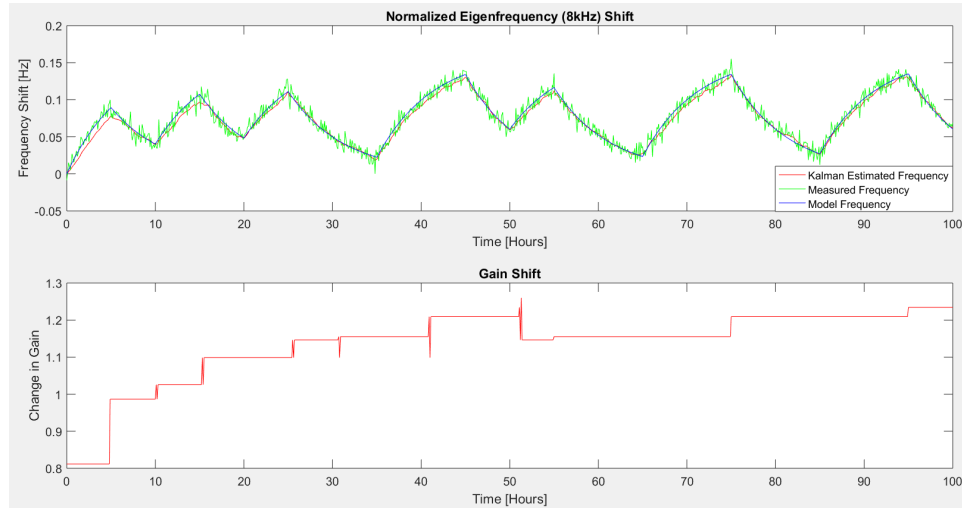


Figure 20: Simulated period of locked and unlocked states where the noisy measurements have a factor >1 applied to the input laser power and the nested Kalman Filter updates itself in a bias towards this noise's behavior. The upper graph depicts alternating locked and unlocked states for a span of 100 hours. The red line is the Kalman Filter Estimate, the green line represents the simulated noisy measurements, and the blue line is the assumed model frequency. The bottom graph depicts in red the change in gain obtained by the updating mechanism of the nested Kalman Filter.

The second case involves encountering noisy measurements where the control parameter, laser power, has an unknown factor less than 1 resulting in a lower gain coefficient in the measurement data. As shown below, the nested Kalman Filter updates itself at the end of locked states to update its gain coefficient. This results in a decrease in the gain and this change in gain is proportional to the coating absorption.

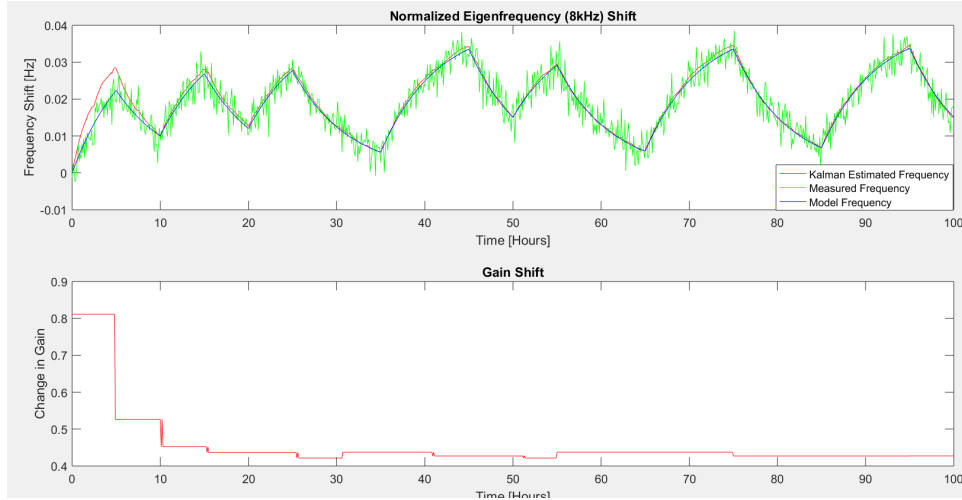


Figure 21: Simulated period of locked and unlocked states where the noisy measurements have a factor <1 applied to the input laser power and the nested Kalman Filter updates itself in a bias towards this noise’s behavior. The upper graph depicts alternating locked and unlocked states for a span of 100 hours. The red line is the Kalman Filter Estimate, the green line represents the simulated noisy measurements, and the blue line is the assumed model frequency. The bottom graph depicts in red the change in gain obtained by the updating mechanism of the nested Kalman Filter.

4 Final Results

4.1 Actual Data Results: July 2017

After completing the nested Kalman Filter and testing it with simulation data, I worked on testing it with IWAVE plot data provided by the researcher Timesh Mistry. IWAVE is a frequency tracking package that we used to estimate eigenfrequencies in real time.

The filter has been tested on two locked periods of IWAVE data for three days of July 2017. These two periods are integrated into a period of simulated locks and unlocks eigenfrequency data. The two periods of actual eigenfrequency data are approximately a day apart and as shown in the graphs below. In order to extract the coating absorption with the available eigenfrequency measurement data, this three day segment of data was run recursively to expand it to a nine day interval. As shown below in figure 28 this rerunning of the data allowed the nested Kalman Filter to update the gain until it reached a leveling point. With this information, the change in gain provides the necessary information to extract the coating absorption.

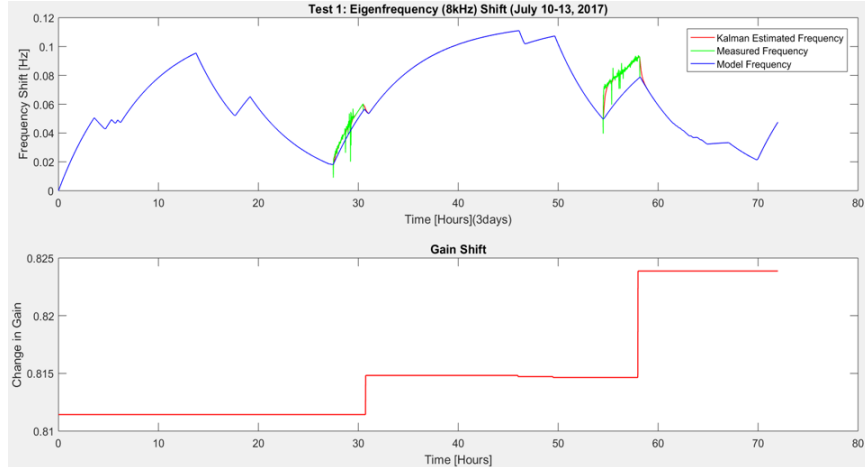


Figure 22: This is testing a 3 day period from July 10-13, 2017 with two locked periods of actual IWAVE data. The upper graph depicts a period of locked and unlocked states where End Test Mass Y is experiencing periods of heating (locked state) and periods of cooling (unlocked state) for a total period of three days. The blue line is the model frequency obtained applying the parameterized model discussed in the thermal modelling section. The nested Kalman Filter is only applied in two locked states illustrated above from approximate ranges of 28-30 hrs and 58-60 hrs. The green line represents the use of actual IWAVE eigenfrequency data for ETMY during the month of July 2017 and the red line represents the output Kalman estimate frequency from the nested Kalman Filter. The bottom graph illustrates the results of the change in gain from the end of the two locked periods monitored applying the nested filter.

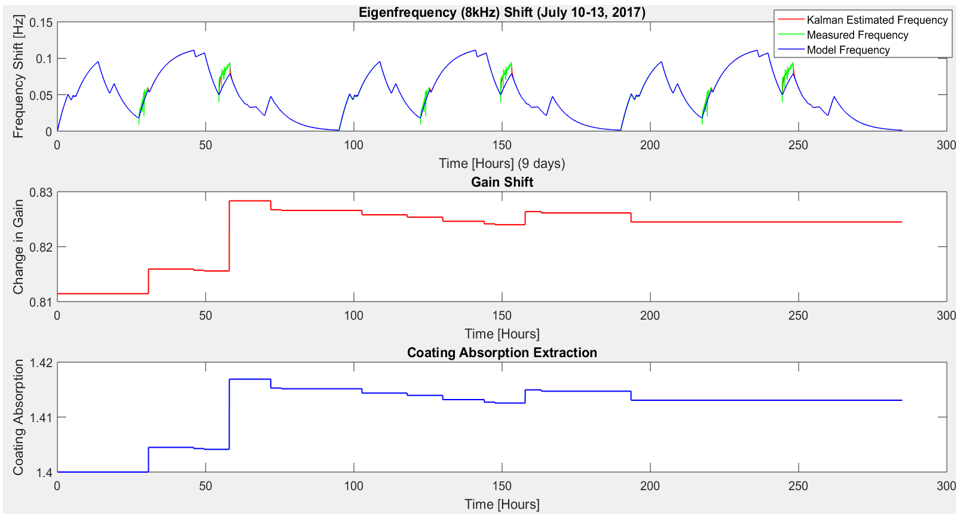


Figure 23: This is a 9 day period repeating the July 10-13, 2017 to apply the Kalman Filter over a longer period of time and observe the change in gain and extract the coating absorption. The upper graph depicts a period of locked and unlocked states where End Test Mass Y is experiencing periods of heating (locked state) and periods of cooling (unlocked state) for a total period of nine days. The blue line is the model frequency obtained applying the parameterized model discussed in the thermal modelling section. The nested Kalman Filter is only applied in 6 locked states. The green line represents the use of actual IWAVE eigenfrequency data for ETMY during the month of July 2017 and the red line represents the output Kalman estimate frequency from the nested Kalman Filter. The middle graph illustrates the results of the change in gain from the end of the two locked periods monitored applying the nested filter. The bottom graph depicts the resulting coating absorption shift over time given its dependence on the change in gain.

The ultimate goal is to test the nested Kalman Filter on actual IWAVE data for the entire month of July 2017, but with the current results it is evident that the actual measurements have another factor dependence. The measurements show that the current assumed model of the system needs to be improved to take into account other factors affecting the behavior of the eigenfrequency change. The assumed model represented above by the exponential in blue requires a rising linear behavior as the measurement data in green begins to diverge from the model over time. This highlights the presence of factors other than input laser power affecting the shift in frequency.

5 Conclusion

In a final analysis, it is evident that Kalman Filters provide useful monitors and can help provide more accurate models of a system. This project centers around building a mirror degradation monitor applying a nested Kalman Filter.

The monitor created utilizes the test masses 8 kHz mechanical eigenfrequencies to probe the test mass temperature. The system uses a first order exponential model derived from finite element analysis. The model is fit from the eigenfrequency response to a 0.1 W step in laser power heating on the HR surface, equivalent to 1ppm absorption of a 100kW beam. The model time constant is 6.3 hours, and has an amplitude of 8.114 Hz/W. The inner Kalman Filter state is the eigenfrequency. The outer Kalman Filter updates the model amplitude state once per lock, this provides an estimate of the coating absorption. The monitor has been tested on simulated data and on eigenfrequency measurements taken during the month of July 2017. The current results provide corroborating evidence for an ETMY absorption of approximately 1.4 ppm. However, the current stage of this project highlights that there are further advancements that can take place.

6 Future Work

Future work that can be completed on this project involve running the filter over longer periods of time with IWAVE data to improve absorption estimate. Challenges that need to be addressed and solved include the presence of noisy IWAVE frequency data and the need to improve the parametric model. As a result, a next step in the project is to remove outliers from the IWAVE frequency data. Moreover, the current finite element model needs to include several other factors including ambient temperature as explained in the introductory section. With the application of more inputs in the system, the numerical data used for the fit of the parameterized model can be refined.

Ultimately, the Kalman Filter can be implemented as a real-time LLO monitoring system to further improve the absorption estimation and other parameter estimations. This project focuses on the time evolution behavior of one eigenmode. In the future, it can be combined with a spatial evolution that takes into account several eigenmodes. This could potentially create a stronger mirror degradation monitor with both a time and spatial evolution.

References

- [1] S. Tait, *An Instantaneous Absorption Estimate of aLIGO Test Masses*. pgs. 1-26 (2018).
- [2] H. Wang, C. Blair, M. Dovalé Alvarez, A. Brooks, M. F. Kasprzack, J. Ramette, P. M. Meyers⁶, S. Kaufer, B. O'Reilly, C. M. Mow-Lowry, A. Freise. , *Thermal modelling of Advanced LIGO test masses..* Class. LIGO Document. 26 Apr (2017).
- [3] S.C. Tait, I.W. Martin, C. Blair, R. Jones Z. Tornasi, A. Bell, J. Steinlechner, J. Hough,S. Rowan. *Optical Absorption of Ion Plated Coatings and Instantaneous absorption at LLO.* <https://dcc.ligo.org/DocDB/0150/G1800531/001/LVC2018.pdf>(2018).
- [4] S. Tait, *Thermal Modelling*. LIGO COMSOL models.
- [5] G. Valdes, *Data Analysis Techniques for LIGO Detector Characterization*. University of Texas at San Antonio (2017).
- [6] Kalman Filter Tutorial, *Water Tank Sample Tutorial*. University of North Carolina (2018).
- [7] COMSOL, *The Heat Transfer Branch*. 709745 ISSN 02608774 (2012).
- [8] A. Brooks, *Pure state space model of thermal effects*. LIGO-T16xxxx-v1-D (2018).
- [9] Mathworks, *Kalman Filter Example*. (2018).
- [10] E. Black, *Notes on the Pound-Drever-Hall technique*. LIGO-T980045- 00- D (1998).
- [11] Abbot B.P., and LIGO Science Collaboration. “Calibration of the Advanced LIGO detectors for the discovery of the binary black-hole merger GW150914.” *Phys. Rev. D*95, 062003 (2017). P1500248
- [12] M. Al-Ahdab, “2D Object Tracking Tutorial with Kalman Filter.” Aalborg University (2016).

7 Appendix

7.0.1 State-Space Representation

I started by defining the position (x), velocity (v), and acceleration (a) of the object and then creating the state space variables. The state space vector is composed of the four variables which were derived from following the four kinematic equations below. [12]

$$x(k) = x(k-1) + t_s v_x(k-1) + \frac{t_s^2}{2} a_x(k-1) \quad \text{Equation 15.}$$

$$y(k) = y(k-1) + t_s v_y(k-1) + \frac{t_s^2}{2} a_y(k-1) \quad \text{Equation 16.}$$

$$v_x(k) = v_x(k-1) + t_s a_x(k-1) \quad \text{Equation 17.}$$

$$v_y(k) = v_y(k-1) + t_s a_y(k-1) \quad \text{Equation 18.}$$

State-vector, X

The state space is represented as:

$$X = \begin{pmatrix} x(k) \\ y(k) \\ v_x(k) \\ v_y(k) \end{pmatrix} \quad (19)$$

State-propagation matrix, A

The state-transition model which is derived by following equations 15-18 and can be expressed as:

$$A = \begin{bmatrix} 1 & 0 & t_s & 0 \\ 0 & 1 & 0 & t_s \\ 0 & 0 & 1 & 0 \\ 0 & 0 & 0 & 1 \end{bmatrix} \quad (20)$$

Control-Input Matrix, B , and Control vector, u

The control input matrix is derived from the acceleration of both the x and y directions and also applies the kinematic equations. The control vector is composed of both the x and y accelerations.

$$B = \begin{bmatrix} \frac{t_s^2}{2} & 0 \\ 0 & \frac{t_s^2}{2} \\ t_s & 0 \\ 0 & t_s \end{bmatrix} \quad u = \begin{bmatrix} a_x(k-1) \\ a_y(k-1) \end{bmatrix} \quad (21)$$

Complete Process Model

The full state-space model for the tracking of a single object becomes: [12]

$$X(k) = \begin{bmatrix} x(k) \\ y(k) \\ v_x(k) \\ v_y(k) \end{bmatrix} = \begin{bmatrix} 1 & 0 & t_s & 0 \\ 0 & 1 & 0 & t_s \\ 0 & 0 & 1 & 0 \\ 0 & 0 & 0 & 1 \end{bmatrix} \begin{bmatrix} x(k-1) \\ y(k-1) \\ v_x(k-1) \\ v_y(k-1) \end{bmatrix} + \begin{bmatrix} \frac{t_s^2}{2} & 0 \\ 0 & \frac{t_s^2}{2} \\ t_s & 0 \\ 0 & t_s \end{bmatrix} \begin{bmatrix} a_x(k-1) \\ a_y(k-1) \end{bmatrix} \quad (22)$$

$$X(k) = AX(k-1) + Bu(k-1) + w \quad \text{Equation 23.}$$

Observation Model, C, and Observations, Z

The observation $Z(k)$ comes from real measurements and C is the observation model. The prediction of the measurement is obtained by utilizing C which maps the state-space into the observation space.[8]

$$C = \begin{bmatrix} 1 & 0 & 0 & 0 \\ 0 & 1 & 0 & 0 \end{bmatrix} \quad (24)$$

$$Z(k) = CX(k) + v \quad \text{Equation 25.}$$

By following the state-space model outlined above and the Kalman Filter algorithm, I created a Matlab script that generates the state space representation of the model and takes in simulated measurement data and control parameter data. It then applies a for loop to extract the Kalman estimate for a given time interval as it goes through both x and y measurements. [12]

Below are two graphs that distinguish the model and the measurements and the measurements with the Kalman Estimation. The model being applied is an assumed model and is not in fact the real model. This is analogous to my project's Kalman filter since I will be utilizing an assumed model that does not behave identically as the real model. A real model is not available to us and as a result we have to parametrize to find the closest match. By using an assumed model and actual measurements, a better estimate of the behavior of the system can be modelled. However, it is crucial to apply the correct process variance as explained in the following section.

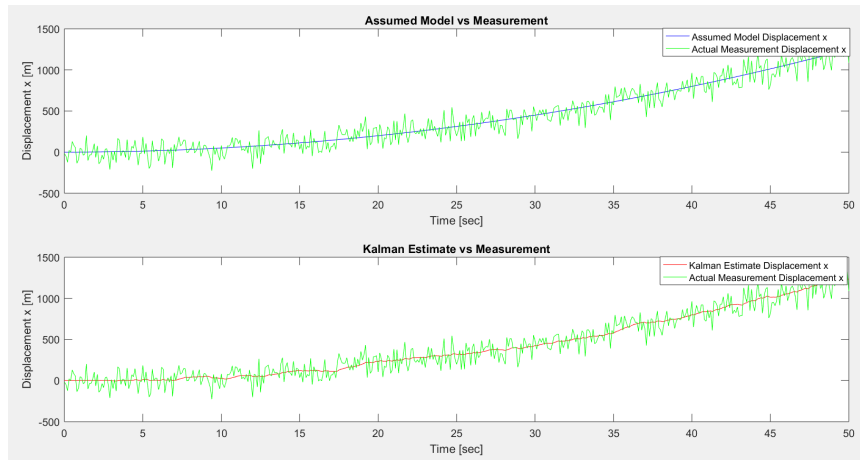


Figure 24: The top graph is a comparison of the assumed object's x -displacement and the actual x -measurement. The bottom graph is a comparison of the object's measured x -displacement and the estimated displacement.

7.0.2 Tuning the Practice Kalman Filter

When setting the Kalman Filter, it is imperative to carefully choose the values for the process variance Q and the measurement variance R . The variance corresponds to the fluctuations of the data and the choice of Q and R all depends on the trust one has on the data. [5]

The figure below illustrates an incorrect process variance known as overfitting where the Kalman estimates confide too much in the measurement data over the assumed model. This problem takes place when Q is significantly greater than R . It results in estimates that contain the measurement noise and that do not provide a better estimate of the behavior of the system.

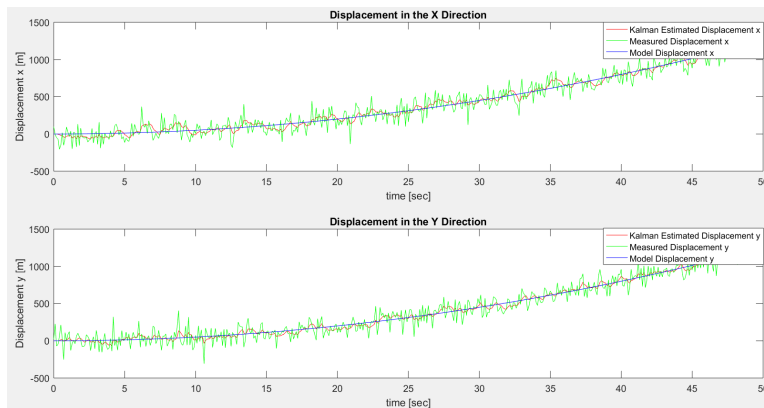


Figure 25: Incorrect process variance leading to an **overfitting** as shown above. The Kalman Estimate trusts the measurements over the model.

Figure 18 depicts another incorrect process variance known as underfitting where the Kalman estimates confide too much in the assumed model data over the actual measurements. This problem takes place when R is significantly greater than Q . This results in estimates that are dominated by the assumptions of the model.

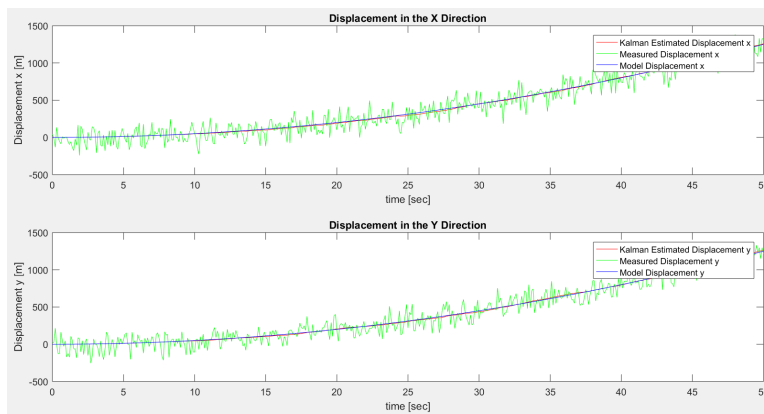


Figure 26: Incorrect process variance leading to an **underfitting** as shown above. The Kalman Estimate trusts the assumed model over the model.

The figure below proves a better fit as it confides in both the measurements and the assumed

model. When setting up a Kalman Filter, it is crucial to carefully decide on the process variance as it controls the behavior of the Kalman estimates.

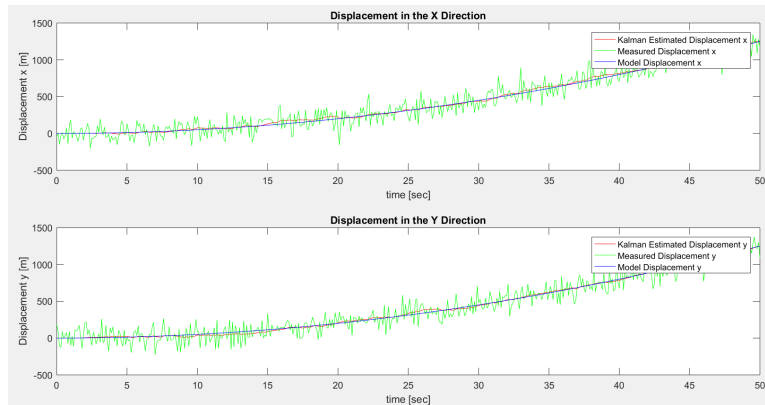


Figure 27: Correct process variance leading to an **good fitting** as shown above. The Kalman Estimate has a balanced trust in both the model and the measurements.

7.0.3 Extracting the Velocity from the Kalman Filter

After completing this practice Kalman Filter, the velocity state space variables for both the x and y direction were extracted. The purpose of this exercise is to see how a state parameter that is not a direct observable, such as coating absorption, might be extracted from the Kalman Filter. The graph below illustrates both velocity graphs of the two directions. Theoretically, if the behavior of the following results were based on the assumed model of the displacement, the velocity would be linear with a positive slope. This is since the displacement was parabolic and concave up. The graphs below are rising and linear regression can be applied to them to obtain the linear equations that best fit the data, but my goal was to transition into working on the project Kalman Filter. These plots were extracted by simply taking the third and fourth state space variables of the state-space representation of the model.

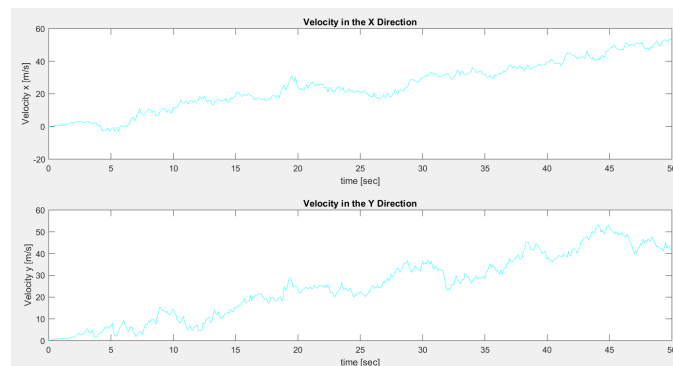


Figure 28: The extraction of both the x and y direction velocities from the state vector of the state-space representation of the system.

8 Code

8.1 Practice Position Tracking Kalman Filter

```

clear
clc
close all
t_i = 0.1; %Defining the sample time

%The State Matrix Below
A = [1 0 t_i 0; 0 1 0 t_i; 0 0 1 0; 0 0 0 1];
%Output Matrix
C = [1 0 0 0; 0 1 0 0];
%B is the Input Matrix
B = [0.5*t_i^2 0; 0 0.5*t_i^2; t_i 0; 0 t_i];
x = [0;0;0;0]; % Initial Conditions

%Defining a system to generate model data
system = ss(A, B, eye(4), [], t_i);

t = 0:t_i:50 %The Time interval

%Below we are assuming the uncertainties in acceleration are all equal
stdax = 10; %standard deviation ax
stday = 10; %standard deviation ay

%In practice (below), these values are determined experimentally

%Defining the input accelerations:
inputax= ones(1, length(t));
inputay = ones(1, length(t));
u = [inputax; inputay];
x0 = [0;0;0;0];
%Now generating the state space representation of the model
Xmodel = lsim(system, u, t, x0);
xmodel = Xmodel(:, 1);
ymodel = Xmodel(:, 2);
velocity_xmodel = Xmodel(:, 3);
velocity_ymodel = Xmodel(:, 4);

%Defining V:
measurement_noise_v= [75.^2 0; 0 75.^2];

%Generating measurement data by adding noise to the modelled data: (This is
%simulation (actual measurement data already has noise))
xm = xmodel + normrnd(0, 100, length(xmodel),1);
ym = ymodel + normrnd(0, 100, length(ymodel), 1);

%Initializing the matrices for the for loop
Xest = zeros(4,length(t));
Xest(:, 1) = x0;

%Defining R and Q
R = measurement_noise_v*C'*C'; %Measurement Noise covariance
Q = [stdax.^2 0 ; 0 stday.^2] %Process Noise covariance

%Initializing P
P= B*Q*B';
for (i =2:1:length(t));
    %Prediction Phase
    %The line below is predicting the error covariance ahead
    P = A*P*A' + B*Q*B'; %Predicting the covariance matrix
    Xest(:,i) =A*Xest(:, i-1)+ B*u(:, i-1); %Predicting the State ahead
    %Correction Phase
    S = C*P*C'+ R
    K = (P*C')/S; % Calculating the Kalman Gain
    %Below I am updating the estimate with the measurement
    Xest(:,i)= Xest(:, i) + K*([xm(i); ym(i)]-C*Xest(:,i)); %Estimating the
    P = (eye(4)-K*C)*P; %This is updating the error covariance which then I
end;

```

8.2 Coating Absorption Simple Kalman Filter

```

clear
clc
close all

t_i = 0.1; % Sample Time



---


%% The Matrix Below is the State Transition Model
Gain= 0.1136/0.14;
Tau = 6.289;
c = 8126;
N = Gain/Tau;
D = 1/Tau;
A = [ 1-D*t_i];



---


%% C is the output matrix: It is the observation model that maps the true
%state-space into the observed space
C = [ 1 ];



---


%% B is the input-control matrix:
B = [ N*t_i ];
f = [0]; %Initial Conditions



---


%% Defining the State-Space Model
system = ss(A, B, eye(1), [], t_i);

t = 0:t_i:10; %The Time Interval (change)



---


%%
%The standard deviation in the control variable
std_laserpower = 0.07;
%% In practice (below), these values are determined experimentally
%Defining the input pow:
inputpower= 0.1*ones(1,length(t)) ;%normrnd(0, std_laserpower, 1, length(t))
u = [inputpower];
f0 = [0];
%% Now generating the state space representation of the model
Fmodel = lsim(system, 2*u, t, f0);
fmodel = Fmodel(:, 1);
%Defining V:
measurement_noise_v= [0.01.^2 ];



---


%% Generating measurement data by adding noise to the modelled data: (This
%simulation (actual measurement data already has noise))
fm = fmodel + normrnd(0, 0.006, length(fmodel), 1);
%dfm = dfmodel + normrnd(0, 50, length(dfmodel), 1);

%Initializing the matrices for the for loop
Fest = zeros(1,length(t));
Fest(:, 1) = f0;



---


%% Defining R and Q
R = measurement_noise_v*C*C'; %Measurement Noise covariance
Q = [std_laserpower.^2 ]; %Process Noise covariance



---


%% Starting Kalman Loop
P= B*Q*B';
for (i =2:1:length(t));
    %Prediction Phase
    %The line below is predicting the error covariance ahead
    P = A*P*A' + B*Q*B'; %Predicting the covariance matrix
    Fest(:,i) =A*Fest(:, i-1)+ B*u(:, i-1); %Predicting the State ahead
    %Correction Phase
    S = C*P*C' + R ;
    K = (P*C')/S; % Calculating the Kalman Gain
    %Below I am updating the estimate with the measurement
    Fest(:, i) = Fest(:,i) + K*(fm(i)-C*Fest(:,i)); %Estimating the State
    P = (eye(1)-K*C)*P; %This is updating the error covariance which then 1
end;

%When setting the input laser power as zero, there should be no change in
%the eigenfrequency since no heat is being applied (unlocked-cooling), when
%in locked state the eigenfrequency experiences an upward shift
subplot(111);
plot(t, Fest(1,:), 'r', t, fm, 'g', t, fmodel, 'b');
xlabel('time [sec]');
ylabel('Frequency Shift Normalized [8 Hz]');
title('Frequency Shift (8 kHz Eigenmode)');
legend('Kalman Estimated Frequency', 'Measured Frequency', 'Assumed Model F

```